Cold-end corrosion in biomass combustion - role of calcium chloride in the deposit

Ruozzi, Alessandro; Vainio, Emil; Kinnunen, Hanna; Hupa, Leena

Published in:
Fuel

DOI:
10.1016/j.fuel.2023.128344

Published: 01/10/2023

Document Version
Final published version

Document License
CC BY

Fuel 349 (2023) 128344

Contents lists available at ScienceDirect

Fuel

journal homepage: www.elsevier.com/locate/fuel

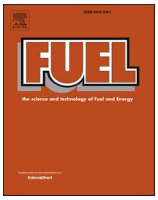

Cold-end corrosion in biomass combustion – Role of calcium chloride in the deposit

Alessandro Ruozzi [a,*], Emil Vainio [a], Hanna Kinnunen [b], Leena Hupa [a]

[a] Johan Gadolin Process Chemistry Centre, Combustion and Materials Chemistry Group, Åbo Akademi University, Turku, Finland
[b] Valmet Technologies Oy, Lentokentänkatu 11, 33900 Tampere, Finland

ARTICLE INFO

Keywords:
$CaCl_2$
Cold-end corrosion
Hygroscopic deposits
Deliquescent salts
Biomass combustion

ABSTRACT

Using sustainable fuels in power production may lead to an increased risk of corrosion of various boiler parts. In biomass and waste combustion, hygroscopic and deliquescent deposits can cause corrosion of, e.g., preheaters and flue gas cleaning equipment. In the colder part of the boiler, calcium chloride ($CaCl_2$) may form when utilizing fuels containing chlorine. Calcium chloride is a deliquescent salt which can absorb moisture from the flue gas leading to the dissolution of the salt itself. When calcium chloride deliquesces, it forms a corrosive electrolyte that can cause severe corrosion. In this work, full-scale corrosion probe measurements in a biomass boiler and laboratory experiments were carried out to study whether calcium compounds and especially $CaCl_2$ might cause corrosion at different temperatures and humidity conditions. The impact of $CaCl_2$ on the corrosion of carbon and stainless steel was studied in more details at various temperatures (80, 100 and 120 °C) and flue gas moisture levels (15–25 vol% H_2O) in a laboratory furnace. Different exposure times were used (24, 72 and 168 h), and the effect of mixtures of $CaCl_2$ and calcium carbonate ($CaCO_3$) was also studied. The corrosion rate was gravimetrically measured, and the sample cross-sections were analysed with SEM-EDX to verify the impact of different elements on the corrosion. Full-scale measurements showed chlorine-induced low-temperature corrosion. The main species in the deposit were calcium and chlorine, and corrosion was observed at conditions at which $CaCl_2$ deliquesces. The laboratory work showed that although the deposit contains mainly calcium carbonate, which is not deliquescent, the highest corrosion rate (>1 mm/year) was found with 5 wt% $CaCl_2$ in the salt deposit mixture. The tests showed that the corrosion rate is linear with time, and severe corrosion of carbon steel occurs when $CaCl_2$ deliquesces. Stainless steel did not show any measurable corrosion at the conditions tested.

1. Introduction

The thermal efficiency of a boiler increases by recovering heat from the flue gas. However, too low material temperatures can lead to cold-end corrosion (also known as low-temperature corrosion) [1]. In fossil fuel combustion, particularly coal, the most critical factor is the sulfuric acid dew point temperature, below which sulfuric acid-induced corrosion occurs [2–4]. In biomass combustion, sulfuric acid is not normally present in the flue gases because the sulfur content of biomass fuels is generally low, and the relatively low temperature converts little SO_2 into SO_3. Furthermore, SO_3 can react with alkalis present in the fuel and form alkali sulfates [2–5]. In biomass combustion, low-temperature corrosion is generally caused by hygroscopic deposits that absorb moisture from the flue gas [1,6–14]. Hygroscopic salts can absorb moisture from the flue gas, leading to a corrosive environment on the steel surface. Deliquescence is the process by which a substance absorbs moisture from the atmosphere until it dissolves in the absorbed water and forms a solution. Deliquescent properties of salts have mainly been studied for aerosols at atmospheric conditions, e.g. [15–20]. The moisture level at which deliquescence occurs is called deliquescence relative humidity (DRH) [1]. However, this paper uses mainly the term deliquescence temperature at a certain water vapour concentration to describe the conditions at which deliquescence occurs. When hygroscopic salts undergo deliquescence, they form a corrosive electrolyte that can cause severe corrosion of various parts of the boiler. Many chlorides are highly hygroscopic, e.g., $CaCl_2$, $ZnCl_2$, and NH_4Cl [1]. The formation of $CaCl_2$ is illustrated in Fig. 1.

Calcium carbonate is introduced into the boiler with the fuel or

* Corresponding author.
E-mail address: alessandro.ruozzi@abo.fi (A. Ruozzi).

https://doi.org/10.1016/j.fuel.2023.128344
Received 15 December 2022; Received in revised form 26 March 2023; Accepted 4 April 2023
Available online 25 May 2023

additives, e.g., limestone used to reduce the emissions of SOx [4]. It has been shown that limestone addition in a CFB boiler leads to the formation of $CaCl_2$ in the boiler cold-end and to an increased corrosion risk [4]. When it is fed into the furnace, $CaCO_3$ forms CaO and CO_2. CaO captures SO_2 to form calcium sulfates. A part of the CaO can deposit in various areas of the boiler, reacting with HCl(g) present in the flue gas to form $CaCl_2$ according to the following reaction [1]:

$$CaO\ (s) + 2HCl\ (g) \rightarrow CaCl_2\ (s) + H_2O\ (g) \quad (1)$$

It has been shown by some authors [21] that the reaction between CaO or $Ca(OH)_2$ and HCl could form both CaOHCl and $CaCl_2$.

The hygroscopic behaviour of $CaCl_2$ at 25 vol% H_2O is illustrated in the example in Fig. 2.

Fig. 2**a** presents the cooling of $CaCl_2$ from 160 °C. As the temperature decreases, $CaCl_2$ starts to form hydrates. The formation of the hydrates depends on the cooling rate [1]. These hydrates, however, are not corrosive, i.e., dry $CaCl_2$ is not corrosive when the conditions are above the deliquescence temperature. As the temperature reaches the deliquescence point of 109 °C, the salt completely dissolves to form an aqueous solution. Below the deliquescence curve, $CaCl_2$ forms a corrosive electrolyte [1]. Fig. 2**b** shows the other way around: $CaCl_2$(aq) is below the deliquescence curve and it is completely dissolved. Above the deliquescence curve, the salt remains dissolved and does not recrystallise until the temperature is higher than the recrystallisation temperature (FFig. 2**b**). Understanding this behaviour of $CaCl_2$ is important to prevent operational problems. During soot blowing, there is a momentary increase in the vol% H_2O in the flue gas, during which the conditions may lead to deliquescence of $CaCl_2$.

$CaCl_2$ is corrosive on carbon steel when water is absorbed by the salt [1]. However, whether $CaCl_2$ is corrosive when the deposit consists mainly of calcium carbonate is unclear. Additionally, the corrosivity of $CaCl_2$ has not been fully assessed with various water vapour concentrations above and below the deliquescence temperature. In this work, the formation of $CaCl_2$ was investigated in a full-scale bubbling fluidized bed (BFB) boiler firing wood-based biomass. The role of $CaCl_2$ on corrosion was further studied in the laboratory to understand the effect of $CaCl_2$ content in the deposit on corrosion and corrosion mechanisms. This work investigates the formation, the deliquescent behaviour, and the operational problems that deliquescent salt $CaCl_2$ can cause in the boiler cold-end.

2. Materials and methods

In this work, the experimental section is divided into two parts: the first one discusses the full-scale corrosion and deposit measurements in a biomass-firing BFB boiler, while the second part utilises laboratory corrosion tests of carbon and stainless steel exposed to $CaCl_2$-$CaCO_3$ mixtures to better understand the impact of $CaCl_2$ on low-temperature corrosion.

2.1. Full-scale measurements

The full-scale measurements were carried out in a bubbling fluidized bed (BFB) boiler (<100 MW_{th}) fired with wood-based biomass. An air-cooled probe was exposed for 5500 h. The probe was located in the flue gas duct after the air preheater, where the flue gas temperature varied between 160 and 180 °C during the measurement period. The location of the probe is presented in Fig. 3, together with a schematic illustration of the probe. The HCl concentration in the flue gases varied between 20 and 40 mg/Nm^3, and the moisture content between 20 and 33 vol%. The HCl and H_2O in the flue gas were measured with the plant's FTIR (Fourier-transform Infrared Spectroscopy). The measurement took place after the stack.

Fuel samples were collected frequently during the measurement campaign. The results of the average of multiple fuel analyses are shown in Table 1. The fuel had elevated chlorine and calcium content compared to e.g., stem wood biomass. The fuel was low in sulfur and high in calcium, and its Ca/S molar ratio was 21.6. Thus, the SO_2-capturing potential of the ash was high, and no SO_2 was detected in the

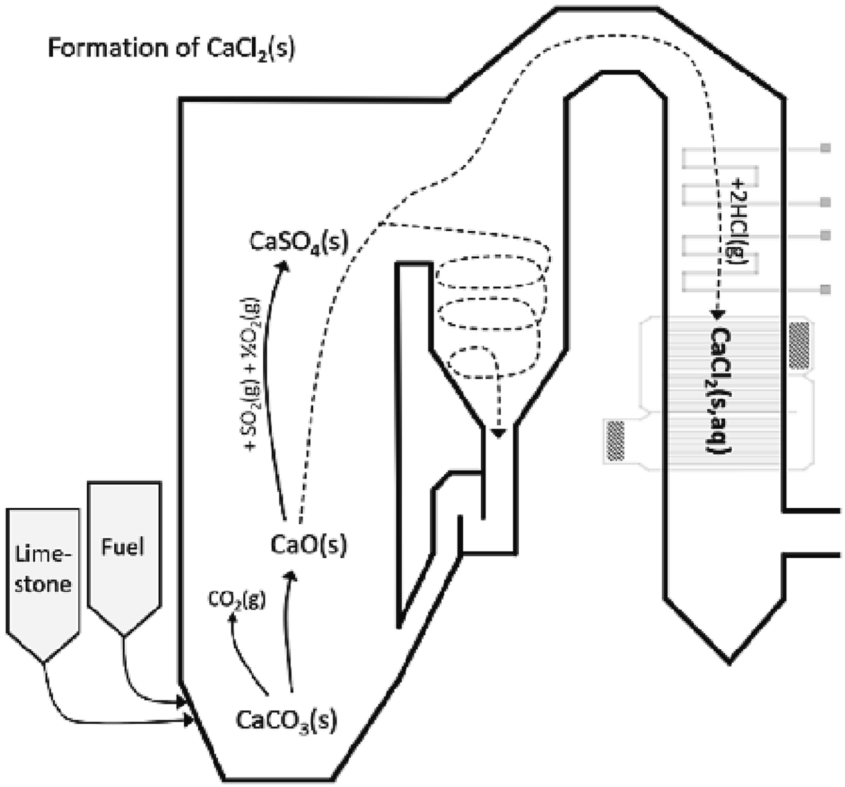

Fig. 1. The formation of $CaCl_2$ in a circulating fluidized bed (CFB) boiler. Picture from Vainio et al. [4].

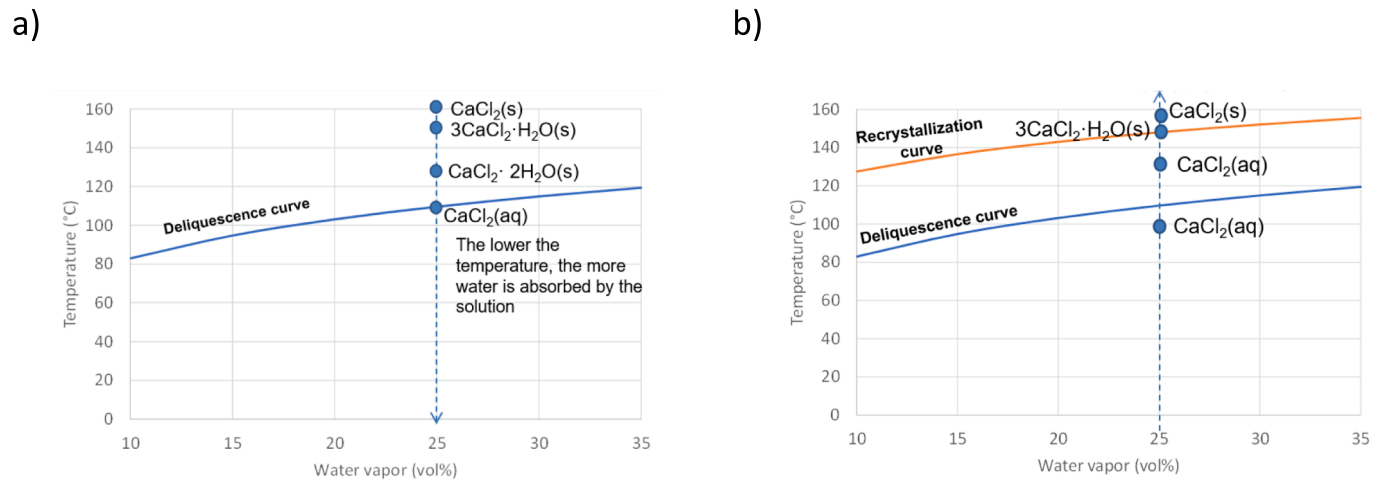

Fig. 2. a) Formation of different hydrates as $CaCl_2$(s) is cooled from 160 °C at 25 vol% H_2O. b) Heating of $CaCl_2$(aq) from 100 to 160 °C at 25 vol% H_2O. The hydrate that is formed depends on the cooling/heating rate. Figure based on data from Vainio et al. [1].

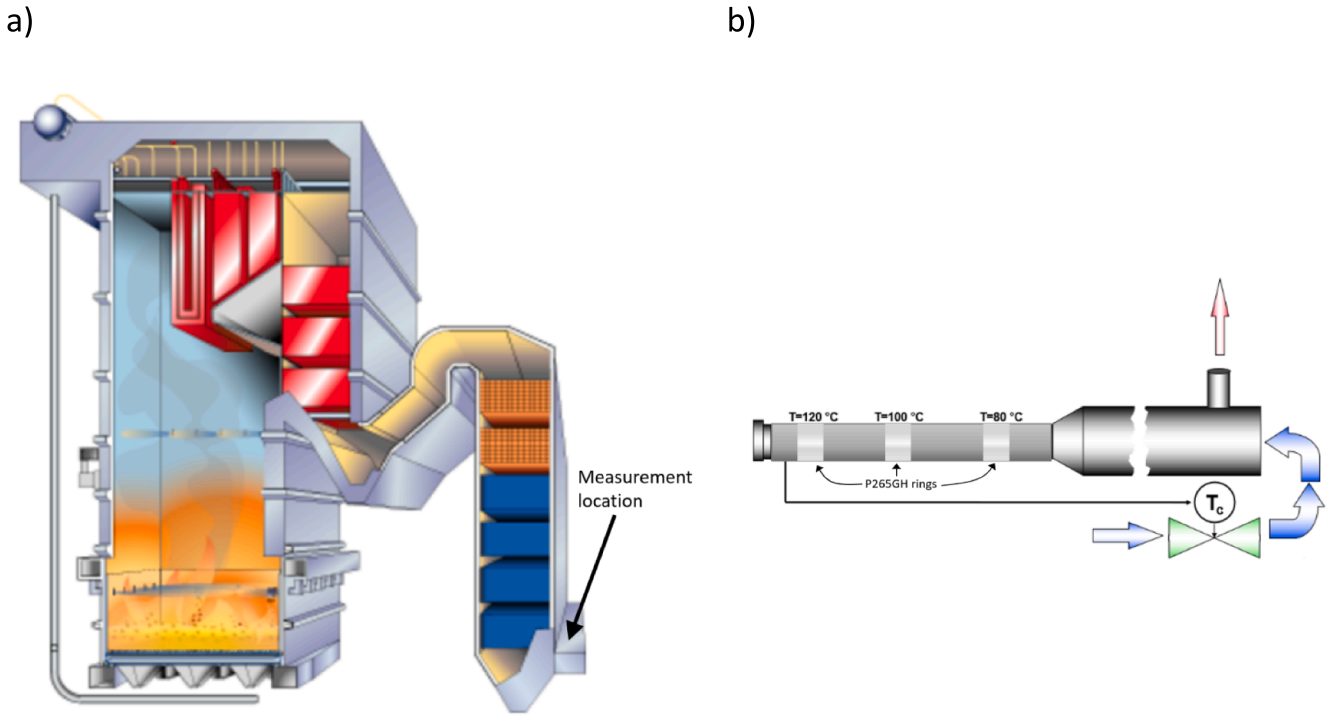

Fig. 3. a) Illustration of the measurement location in a BFB boiler. The probe was located after the air preheaters (indicated with an arrow in the figure). b) Schematic of the air-cooled corrosion probe used in the full-scale measurements.

Table 1
Average fuel composition (d.s. = dry solids).

	Unit	Average
Moisture	%	8.6
C	wt% d.s.	43.8
H	wt% d.s.	5.4
N	wt% d.s.	0.4
S	wt% d.s.	0.05
Cl	wt% d.s.	0.14
Ash, 815 °C	wt% d.s.	9.9
Ca	wt% d.s.	1.35
K	wt% d.s.	0.36
Na	wt% d.s.	0.1
S/Cl	molar ratio	0.4
Ca/S	molar ratio	21.6

flue gases. The low S/Cl and high Ca/S molar ratios indicate the formation of alkali and alkaline earth chlorides. The samples were dried to avoid mould growing before sending them to the analysing laboratory. This drying explains the low analysed fuel moisture (Table 1). The typical moisture content of this type of fuel is > 35 wt%.

Table 2
Material temperatures and average flue gas temperature during the 5500-hour measurement period. (*during shut-down).

Ring	Material	setpoint T	Avg. T_{mat}	Max T_{mat}	Min T_{mat}	Avg. $T_{flue\ gas}$
1	Carbon	120	116	126	70*	171
2	steel	100	104	113	69*	
3	P265GH	80	87	93	69*	

The test rings on the corrosion probe were exposed to three different temperatures, the set points were 80, 100 and 120 °C (Table 2). However, the actual temperature could differ up to 13 degrees from the setpoint. Additionally, there was a 24-hour shut-down in the middle of the testing period. The boiler was brought down and started up again according to the standard operational instructions. The boiler was started up with light fuel oil followed by solid fuel feeding. Thus, the material temperatures were < 80° C for 10–12 h during the shutdown. The exposure time of the corrosion probe was 5500 h. Carbon steel (P265GH) was used as the test material.

The average wall thickness losses were determined for each test ring with a specific micrometre. An example of material loss of the rings is illustrated in Fig. 4.

The corrosion rate was calculated by linear extrapolation of the yearly material loss. In addition, SEM-EDX analyses were carried out on wind-side deposits collected from the corrosion probe (Fig. 5).

2.2. Laboratory corrosion experiments

2.2.1. Chemicals/Hygroscopic salts

Salts used in the laboratory corrosion experiments were $CaCl_2$ (Sigma-Aldrich, anhydrous ≥ 97 %) and $CaCO_3$ (Honeywell, ≥99.0 %). Citric acid was used to wash the salt deposits from the steel surfaces after the exposures. Deionised distilled water was used in the steam generator. Ethanol was used to polish the samples with the finest grit paper.

2.2.2. Corrosion exposures

The corrosion tests were performed in a tube furnace at 80, 100 and 120 °C. A steady and controlled flow of water vapour was produced with a Cellkraft P-2 precision steam generator. The water vapour concentrations used in the corrosion tests were 15, 17, 20 and 25 vol% H_2O, the O_2 concentration was 5 vol% and the rest N_2. These levels of water vapor are similar to the ones that are typically measured in a boiler. The test conditions are illustrated in Fig. 6.

In the tests at 80 °C, the conditions were well below the deliquescence curve (Fig. 6) thus the salt can absorb moisture from the flue gas and form a corrosive electrolyte. In the tests at 100 °C the conditions were close to the deliquescence curve. At 100 °C a narrower range of water in the gas was chosen to study the behaviour of $CaCl_2$ in proximity of the deliquescence curve (Fig. 6). In the tests at 120 °C, no absorption of free water occurs because the conditions are above the deliquescence curve (Fig. 6). However, the salt remains wet if it absorbs water (e.g., during a soot blowing). Thus, the salt mixtures were prewetted to simulate a soot blowing period with high water vapour. The 100 mg salt

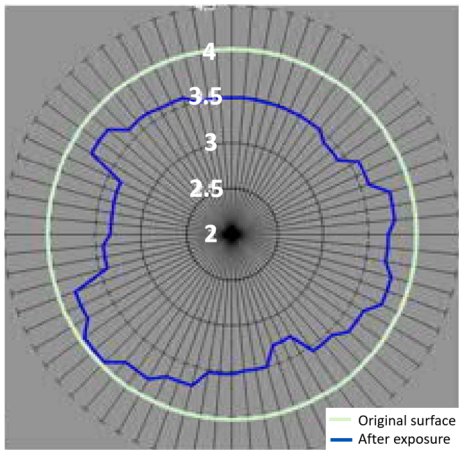

Fig. 4. Material loss of the carbon steel ring used in the full-scale measurement at 120 °C. The wind side is the upper part of the figure. The whole circumferences (360°) of each test ring were measured at 15° intervals. The material loss was relatively evenly distributed around the test rings.

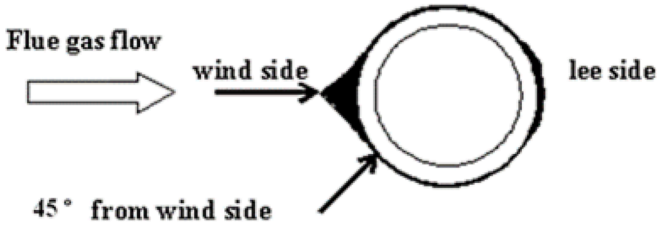

Fig. 5. Illustration of the wind, side, and leeward deposits on the corrosion probe.

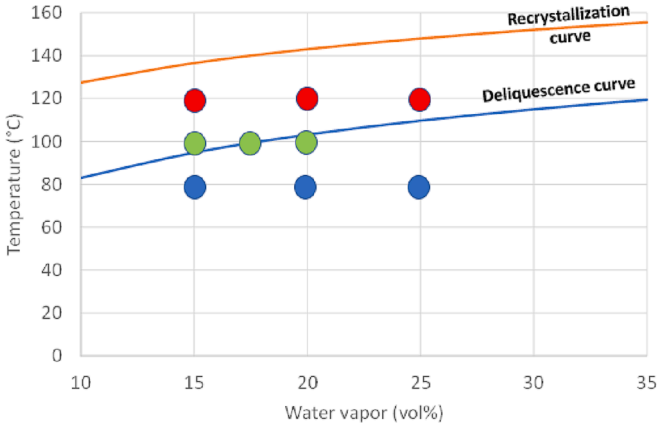

Fig. 6. The blue dots represent the test at 80 °C, the green ones the tests at 100 °C and the red ones the tests at 120 °C. The salt mixtures were prewetted in the tests at 100 °C (at 15 and 17 vol% H_2O) and 120 °C (at all three water vapour levels) just before being inserted into the furnace. The duration of the tests at 100 and 120 °C was 72 h. The duration of the tests at 80 °C varied: 2, 24, 72 and 168 h. (For interpretation of the references to colour in this figure legend, the reader is referred to the web version of this article.)

deposits were prewetted with 2 droplets of deionized water (approximately 0.05 ml per droplet). This amount of added water is more than enough to establish equilibrium between the salt solution and gas phase when the samples were inserted into the furnace [1]. Adding two droplets of water to 100 mg of $CaCl_2$ results in a molality of about 9 of the formed solution. The molality of the metastable solution in the experiments is higher than [1] meaning that some water evaporated from the solution. The prewetting was done just before the insertion of the samples in the furnace. $CaCl_2$ dries if the conditions are above the recrystallization curve (Fig. 6).

The sample holder used in the furnace exposures can host up to 8 samples (Fig. 7**a and 7b**). Thus, different materials and salt mixtures could be tested simultaneously. Depending on the experiment, one or two samples were chosen for SEM-EDX analysis while the remaining ones were used to calculate the average corrosion rate. The sample holder is equipped with three thermocouples (one in the middle and two at the ends) to record the temperature variations during the whole experiment. The temperature difference was approximately ± 1.5 °C, e.g., if the thermocouple in the middle measures 80.0 °C, then the thermocouples at the ends would measure 81.5 °C and 78.5 °C.

The corrosion tests were performed using 20 mm × 20 mm or 20 mm × 17 mm coupons of carbon steel and stainless steel (Table 3).

The coupons were initially polished in water with P120 grit silicon carbide (SiC) paper, then with P320 grit silicon carbide paper and finally with P1000 grit paper in ethanol. Approximately 100 mg of the dry salt mixture was placed on each coupon. $CaCl_2$ is very hygroscopic and it readily absorbs moisture from the surrounding atmosphere. Therefore, the salt mixtures were kept at 60–80 °C and low humidity during storage. The heated salts were mixed and grinded in a heated mortar with a heated pestle. Approximately 100 mg of the dry salt or salt mixture was

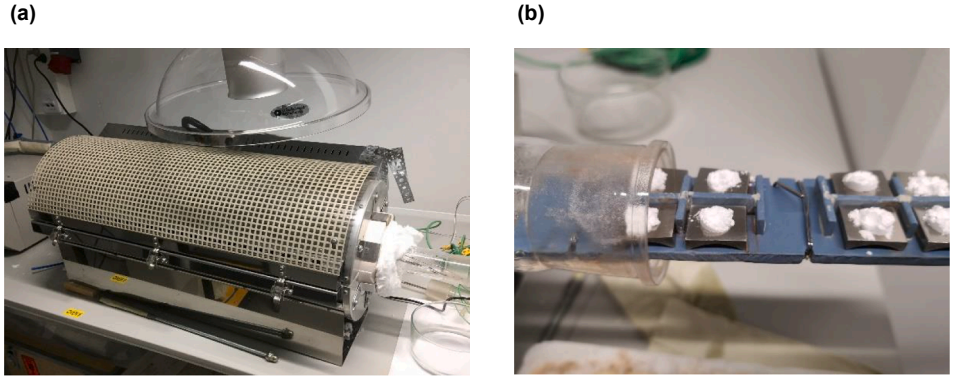

Fig. 7. a) The furnace that was used for the corrosion tests in the laboratory. b) The sample holder before being inserted in the furnace. Up to eight coupons could be tested at the same time. The sample holder was equipped with three thermocouples (one in the middle and two at the ends) to monitor the temperature difference between the extremes during the test.

Table 3
Typical compositions (main elements) of the steel grades used in this study (numbers in wt%).

	Fe	C	Mn	Si	Cr	Ni
P235GH	>97.7	0.16	≤1.2	≤0.35	≤0.3	≤0.3
P265GH	>97.4	0.2	≤1.4	≤0.4	≤0.3	≤0.3
AISI304L	66.8–71.5	0.03	2.0	1.0	17.5–19.5	8–10.5

placed on preheated metal coupons just before inserting them into the furnace. Fig. 8 illustrates the cylindrical glass that was used to pour the salt mixture on the coupons (Fig. 8**a**), and a typical salt layer before (Fig. 8**b**) and after the exposure (Fig. 8**c**).

After the furnace exposure, the salt and corrosion layer were removed by citric acid in an ultrasound bath until all corrosion products were taken away. The total duration of the ultrasound bath in citric acid was approximately 20-minute long. The ultrasound bath was divided in 5-minute-long intervals. At the end of each interval, the sample was weighted to measure the mass loss after each bath. When the corrosion layer was removed, a mass loss was no longer observed between the ultrasound baths. A blank reference sample was used in the acid step to determine the metal loss. The mass loss was determined gravimetrically, and the corrosion rate (mm/year) was calculated by linear extrapolation to estimate the yearly material loss. The experimental matrix is shown in Table 4**.**

The first laboratory experiments studying the impact of $CaCl_2$ on low-temperature corrosion were carried out exposing carbon steel at 80 °C. The exposures were done with 15 and 25 vol% H_2O for 2, 24 (these durations are not mentioned in Table 4) and 168 h to determine how the corrosion rate varies with the exposure time. Based on these experiments, the two steels and salt mixtures were exposed at different temperatures and vol% H_2O for 72 h, as listed in Table 4**.** The 72-hour experiments (see Fig. 6) were performed at different humidity levels (between 15 and 25 vol% H_2O) and temperatures (80, 100 and 120 °C).

Table 4
Salt mixtures, exposure times and humidity levels for the corrosion tests on carbon steel (P235GH) and stainless steel (AISI304L) in the laboratory furnace. The 72-hour tests were performed at 80, 100 and 120 °C. The 168-hour tests were performed at 80 °C.

Steel material	**$CaCl_2/CaCO_3$ (w/w)**					Time (hours)	**Humidity** (vol% H_2O)
	100/0	25/75	50/50	5/95	>99 % $CaCO_3$		
Carbon steel	x	x		x		72	15–25
Stainless steel	x	x				72	15–25
Carbon steel	x		x	x	x	168	20

Furthermore, carbon steel was exposed to Ca-salts mixtures for 168 h (Table 4). The water vapor level was 20 vol% during the 168-hour tests. A test at 80 °C and 20 vol% H_2O was done using $CaCO_3$ (>99 % $CaCO_3$ with some impurities) salt to observe the corrosivity of calcium carbonate on carbon steel (Table 4).

The metal surface and the corrosion products were analysed using a scanning electron microscope with energy-dispersive X-ray spectroscopy (SEM-EDX, LEO 1530 Gemini) to study the corrosion mechanism at the steel-surface interface. Following the furnace experiments, selected samples were encapsulated in epoxy resin and later cut to be analysed. The salt deposit was not washed away, it was rather encapsulated in the epoxy resin so that it was possible to obtain a cross section SEM image of the corrosion layer and the salt deposit on top of it. To prevent water uptake from the atmosphere by the salt, the samples were stored in a desiccator with N_2 or in vacuum before analysis. The samples were stored in a custom-made desiccator filled with nitrogen and silica gel desiccant. No water was absorbed by the salts during storage in the

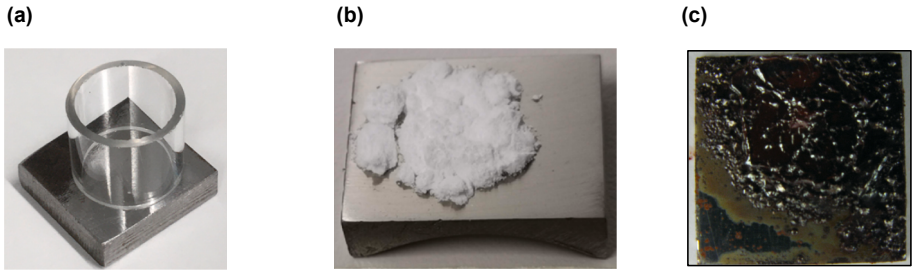

Fig. 8. a) The cylindrical glass used to pour the salt mixture on the heated sample. b) The salt deposit (100% $CaCl_2$) before exposure. c) The salt deposit (100% $CaCl_2$) a few minutes after exposure (at 80 °C and 15 vol% H_2O), showing the appearance after some drying.

vacuum or in the custom-made desiccator. Preventing water uptake proved to be tricky as $CaCl_2$ is very hygroscopic and some water was absorbed when transferring the sample to the SEM. The samples were stored for approximately-one month prior to SEM analysis.

3. Results and discussion

3.1. Full-scale measurements

Wall thicknesses of the probe rings were measured before and after the exposures with a micrometre. The deposits were removed mechanically from the rings, and the corrosion rate was calculated by linear extrapolation to give the yearly material loss. Carbon steel had suffered from heavy corrosion and the corrosion rate was higher at lower temperature.

The boiler was brought down during the measurement therefore the material temperature dropped below 80 °C for 10–12 h. However, this is not believed to have significantly affected the corrosion rate. The maximum calculated annual corrosion rate of 1.8 mm/year was observed for the lowest temperature (87 °C) (Table 5). At 104 and 116 °C, the corrosion rates were 1.4 and 1.1 mm/year, respectively.

In addition to the steel wall thickness measurements, the deposits were analysed with SEM-EDX. The deposits were scraped off from the wind-side of the ring (Fig. 5). The elemental compositions of the deposits are presented in Table 5. The values are averages of three areas. The variations between the three areas were very small. The dominating elements in the deposits were chlorine, calcium, and potassium. In addition, sulfur and sodium were detected. No clear temperature dependence can be seen in the elemental compositions. However, the presence of chlorides seems evident at all tested temperatures. Calculating potassium and sodium as chlorides gives a surplus of chlorine. This suggests the presence of $CaCl_2$ together with $CaCO_3$, $CaSO_4$, CaO and/or $Ca(OH)_2$. However, no analysis verifying the presence of $CaCl_2$ or the calcium compounds was done due to the hygroscopic nature of $CaCl_2$. The formation of $MgCl_2$ in the deposit is also possible.

Table 6 shows the content of different elements in the fly ash collected in the baghouse filter. The chlorine content in fly ash (Table 6) is lower than the one in the deposits collected from the rings (Table 5).

The maximum water vapour content in the flue gases during the measurements was 33 vol%. Using **Equation (1)** from Vainio et al. [1], gives the deliquescence temperature of 118 °C at 33 vol% H_2O. This is an empirical equation to obtain the deliquescence temperature of $CaCl_2$ in the water vapor range of 10–35 vol%.

$$T_{deliquescence,CaCl2} = 29.10 \ln(pH_2O) + 150.0 \text{ (Equation 1) [1]}$$

Severe corrosion may occur below that temperature [1]. The average material temperature (Table 2) in all boiler measurements was below the deliquescence temperature, thus suggesting corrosion induced by $CaCl_2$. Potassium chloride is not deliquescent at these conditions.

Fig. 9 shows a cross-sectional SEM image of the carbon steel (P265GH) ring surface and the corrosion layer that had formed at the average temperature of 87 °C during the full-scale measurements. The image does not suggest any pitting corrosion but rather a significant general corrosion and attack along the grain boundaries in the steel. The image also shows the locations of the EDX analyses of the deposit (spots 1–4), steel surface (spot 5) and steel (spot 6). In spot 1 Ca is probably present as oxide or hydroxide. The elemental analyses are given in Table 7. Iron is present in all points. Sulfur is low or not present at all. All other points but spot 6 (steel) show the presence of chlorine. This implies that chlorine and the deliquescence of $CaCl_2$ in the deposit have been involved in the observed corrosion.

Table 6
Fly ash data in the baghouse filter obtained with ICP-OES (Inductively Coupled Plasma Optical Emission spectroscopy).

	Average content (in w%/w)				
Element	Sample 1	Sample 2	Sample 3	Sample 4	Sample 5
Cl	6.07	1.82	1.6	0.77	0.3
Ca	13	18	19	12	17
K	6	3.8	3.6	4	3.3
Na	1.3	1.18	1.55	1.16	1.15
Si	13.5	20.1	21.5	28.9	22.2

3.2. Laboratory corrosion tests results

3.2.1. The impact of exposure time at 80 °C

Two sets of tests were performed in a laboratory furnace with $CaCl_2$ salt on carbon steel (P235GH) at 80 °C and either 15 vol% or 25 vol% H_2O in the gas to assess the material loss caused by corrosion (Fig. 10). In both cases, the temperature and humidity conditions were well below the deliquescence curve (Fig. 6), i.e., conditions in which $CaCl_2$ absorbs water from the surrounding atmosphere.

The aim was to investigate whether the corrosion rate is linear with time. The measured mass loss of the samples after different exposure times (2, 24 and 168 h) suggested that the corrosion rate increased almost linearly with time (Fig. 10). Similar results indicating that the corrosion rate increased linearly with exposure time were obtained in the tests at 25 vol% H_2O. Therefore, an intermediate duration of 72 h was chosen for the further tests.

3.2.2. The impact of temperature

3.2.2.1. Corrosion at 80 °C. At 80 °C, three tests on carbon steel and stainless steel were carried out with 15, 20 and 25 vol% water vapour in the flue gas (see Table 4). All three water vapor levels were below the deliquescence curve. Therefore, $CaCl_2$ present in the deposit can absorb moisture from the surrounding atmosphere and form a corrosive electrolyte (Fig. 6). Stainless steel never showed any sign of corrosion; therefore, the corrosion rates (illustrated in Fig. 11**a**) refer to carbon steel only. Fig. 11**b** shows the appearance of the different salt mixtures after the exposure at 25 vol% H_2O. It has to be pointed out that stainless steel may suffer from pitting corrosion in the presence of chlorides [12]. However, this was not observed in the tests of the current study. Due to the deliquescence of $CaCl_2$, corrosion occurred on all carbon steel samples. Surprisingly, the salt deposit that proved to be more corrosive was the one containing just 5 wt% $CaCl_2$. This could be explained by the fact that the salt mixture comprising 5 wt% $CaCl_2$ did not form a solution but rather a semi-wet deposit (see metal coupons after exposure in Fig. 11**b**). This could improve the oxygen diffusion to the steal surface.

Table 5
Average temperature of the corrosion probe rings during the full-scale measurements (°C), elemental composition of wind side deposits (atomic %) on the rings, and calculated corrosion rate (mm/year).

Ring	Temp (°C)	Elemental composition (atomic %)										Corrosion rate (mm/year)	$\frac{(K+Na)}{Cl}$ Atomic ratio
		O	Na	Mg	Al	Si	S	Cl	K	Ca	Mn		
1	116	64.6	1.4	1.5	1.2	2.0	5.9	5.7	2.8	14.4	–	1.1	0.74
2	104	59.0	1.7	2.5	–	1.5	1.5	10.6	5.4	15.2	–	1.4	0.67
3	87	65.0	2.3	2.6	1.5	1.8	1.4	5.9	0.4	18.1	0.2	1.8	0.46

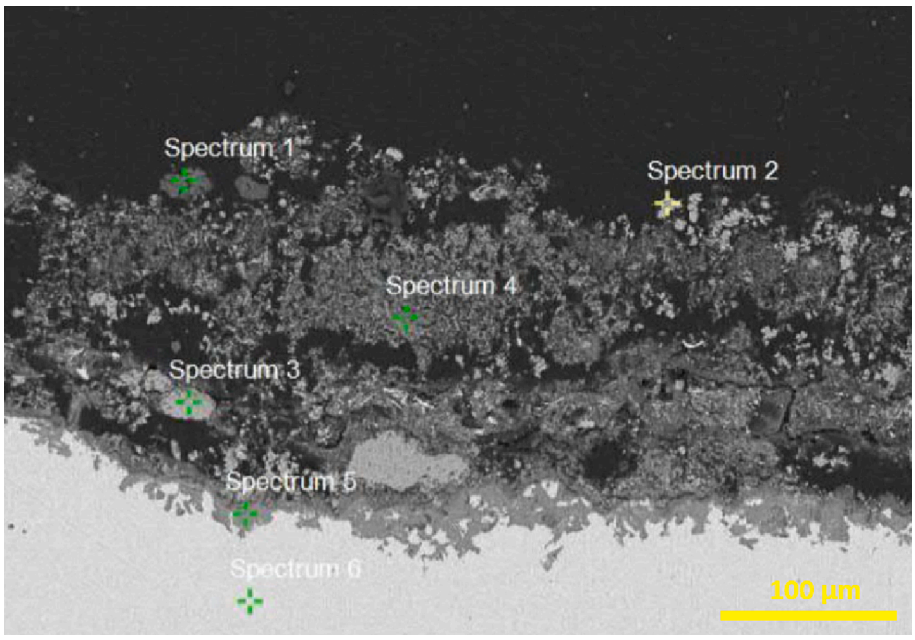

Fig. 9. SEM image of the cross-section of the wind side of the carbon steel (P265GH) corrosion probe ring. The image shows the steel surface and the corrosion layer on top. The ring was exposed in the full-scale boiler for 5500 h at an average temperature of 87 °C (see Table 2).

Table 7
Elemental composition of selected spots of the corrosion layer in Fig. 9 (atomic %).

Spot	O	Na	S	Cl	K	Ca	Mn	Fe
1	71.0	0.2	0.1	1.6	0.1	25.6	0.1	1.2
2	60.7	0.1	0.1	1.1	0.3	0.1	0.3	37.2
3	67.4	0.1	0.0	0.5	0.0	0.0	0.1	31.8
4	58.0	0.1	0.1	1.0	0.1	0.2	1.0	39.5
5	58.6	0.1	0.0	0.6	0.1	0.0	0.1	40.2
6	0.0	0.0	0.1	0.0	0.1	0.0	0.6	99.3

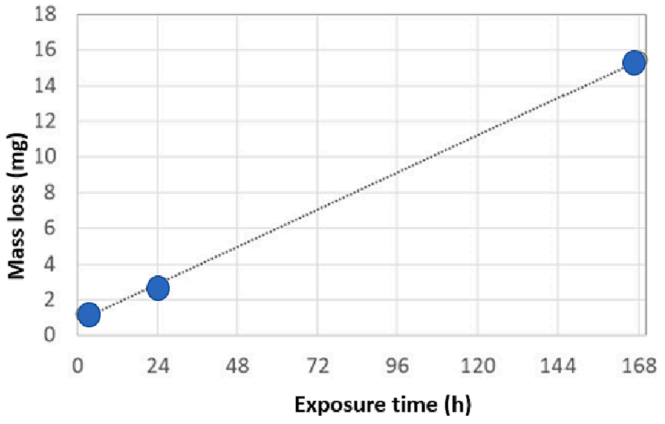

Fig. 10. Average mass loss (blue dots) of carbon steel samples after three exposure times (2, 24 and 168 h) at 80 °C. The flue gas composition was 15 vol % H_2O, 5% O_2 the rest N_2. (For interpretation of the references to colour in this figure legend, the reader is referred to the web version of this article.)

3.2.2.2. Corrosion at 100 °C. At 100 °C, the corrosion of the steels was studied for the Ca-salts mixtures given in Table 4 and the flue gas containing 15, 17 and 20 vol% H_2O for 72 h (see green dots in Fig. 6). At 15 vol% H_2O, i.e., $CaCl_2$ is just above the deliquescence curve. Therefore, the salt does not absorb moisture from the flue gas, and it is not corrosive. As the conditions were in between the deliquescence and the crystallisation curves for $CaCl_2$, the salt deposits were prewetted with distilled water droplets in the tests at 15 and 17 vol% H_2O (see Fig. 6). The measured corrosion rates for carbon steel are shown in Fig. 12**.** No corrosion was measured for the stainless steel samples in these conditions.

The corrosion rates were significantly lower at 100 °C than at 80 °C (see Fig. 11**a**). This is likely attributed to the limited oxygen solubility in the supersaturated salt solution, thus decreasing the corrosiveness of the solution [22]. The same effect of lower corrosion rate for metastable supersaturated solutions of $CaCl_2$ have been reported for 25 vol% H_2O at 120 °C [1]. For the experiments at 100 °C a narrower range of water vapor in the gas (15, 17 and 20 vol% H_2O) was chosen compared to the one used in the furnace tests at 80 and 120 °C (15, 20 and 25 vol% H_2O). The purpose of choosing a narrower range was to study the behaviour of $CaCl_2$ when the conditions are very close to the deliquescence curve (Fig. 6). In a full-scale boiler, fluctuation of the water vapor content, during e.g., soot blowing, could lead to deliquescent conditions at a given temperature. The furnace experiments at 100 °C have shown that the corrosion rate doesn't vary significantly in this narrower range of water vapor content in the gas when salts have been prewetted at 15 and 17 vol% H_2O.

3.2.2.3. Corrosion at 120 °C. The tests at 120 °C were carried out at 15, 20 and 25 vol% H_2O. The conditions were above the deliquescence curve (see red dots in Fig. 6), indicating that $CaCl_2$ does not absorb water and thus is not corrosive. As the conditions were between the deliquescence and recrystallization curves $CaCl_2$ does not deliquesce. In these experiments, the salts were prewetted before the exposures (see Fig. 6). As for the experiments at 80 and 100 °C, no sign of corrosion was found on the stainless steel samples. The corrosion rates for carbon steel are illustrated in Fig. 13.

At 120 °C water vapour seemed to affect the corrosivity more than the other parameters (Fig. 13), and the highest corrosion rates were found at 25 vol% H_2O.

3.2.3. Corrosion after 168 h (one week)

One-week tests on carbon steel were performed at 80 °C and 20 vol% H_2O (see salt mixtures on Table 4) and the results are presented in Fig. 14**a**. As in the 72-hour tests, the salt deposit containing 5 wt% $CaCl_2$

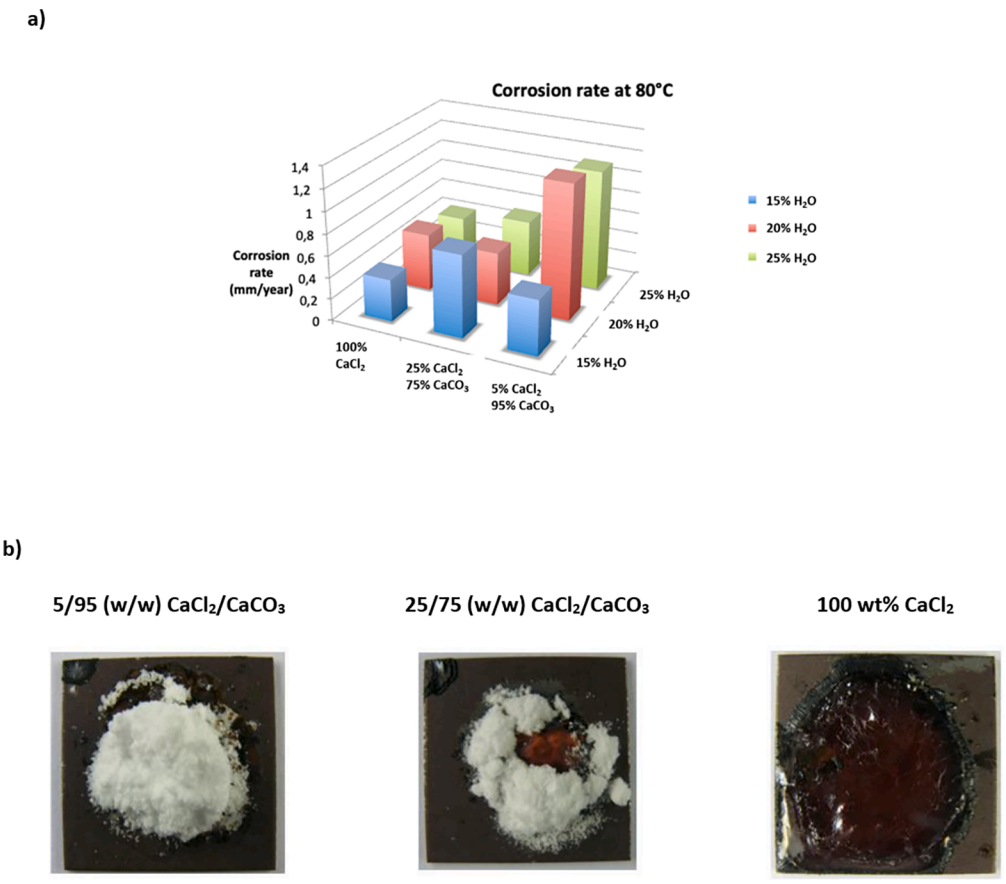

Fig. 11. a) Average corrosion rates (mm/year) of carbon steel (P235GH) after exposure at 80 °C to different calcium salts mixtures. The tests were performed at various water contents in the gas (15, 20, and 25 vol%) for 72 h. b) Pictures of the three salt mixtures taken a few minutes after the exposure at 25 vol% H_2O. A semi-wet solution had formed in the two deposits comprising 5 and 25 wt% $CaCl_2$ due to the lower amount of deliquescent $CaCl_2$ in the mixture.

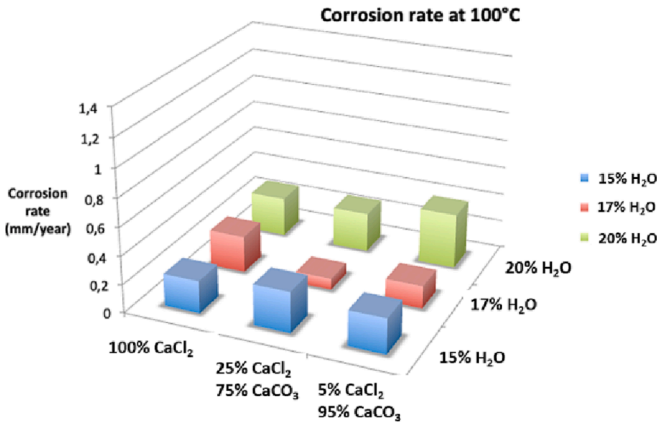

Fig. 12. Average corrosion rates (mm/year) of carbon steel (P235GH) after the furnace tests at 100 °C. The exposure time was 72 h. The Ca-salts mixtures were prewetted just before the furnace exposures at 15 and 17 vol% H_2O.

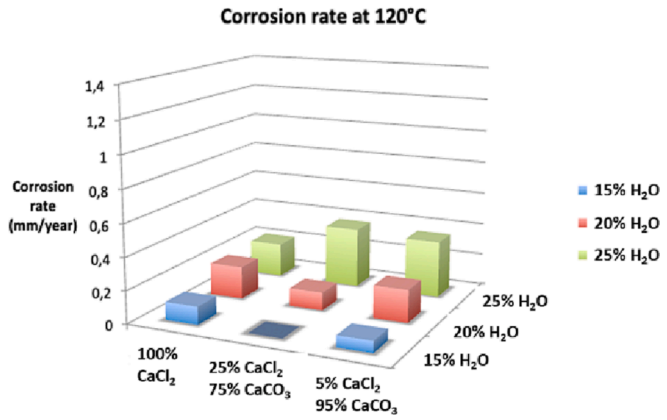

Fig. 13. Average corrosion rates (mm/year) of carbon steel (P235GH) exposed to different mixtures of calcium salts at 120 °C and various water vapour concentrations (15/20/25 vol% H_2O) for 72h. All the salt deposits were pre-wetted just before the furnace exposures.

was the most corrosive and a solution had not formed on the surface of the sample but rather a semi-wet salt. The high corrosion rate for the 5 wt% $CaCl_2$ could be explained by the improved oxygen diffusion in the semi-wet deposit since a solution covering the steel surface had not formed (Fig. 14**b**). Whereas in the other cases the salt solution was covering the whole surface (see the 100 wt% $CaCl_2$ deposit in Fig. 11**b**). Furthermore, the corrosion rate was comparable with the 72-hour test, thus confirming the corrosion rate was linear with the exposure time.

As shown in Fig. 14**a**, the deposit consisting of 99 % $CaCO_3$ also caused minor corrosion. This was a surprise because $CaCO_3$ is not hygroscopic and should be relatively inert. The calcium carbonate used in the experiment was later analysed using ion chromatography, and traces of chlorine (20 ppm) were found. Also, the corroded spots on the steel surface were analysed with SEM-EDX and proved to be enriched in chlorine. This suggests that chlorine can cause corrosion even at extremely low concentrations. In future, purified $CaCO_3$ deposits will be used to verify whether calcium carbonate is corrosive per se.

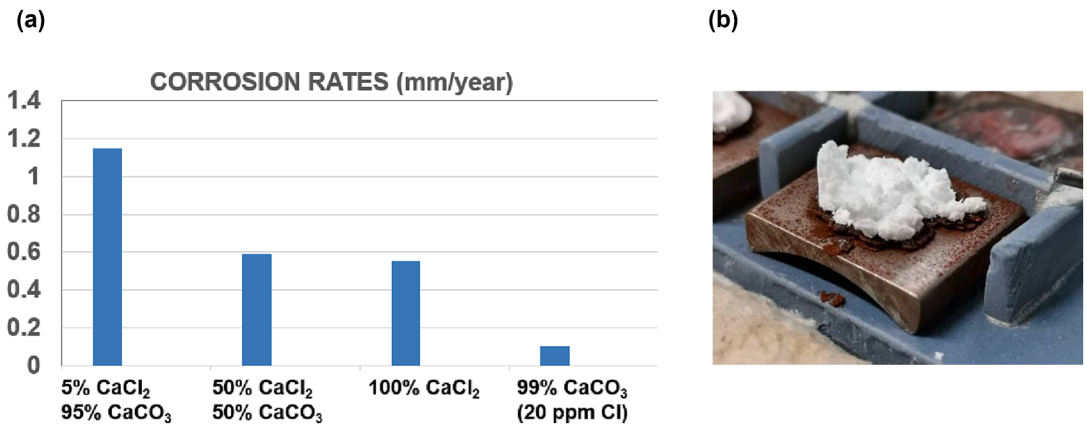

Fig. 14. a) Average corrosion rates for carbon steel (P235GH) exposed to different Ca-salts mixtures at 80 °C and 20 vol% H_2O for 168 h. The 99 wt% $CaCO_3$ salt contained Cl impurities causing the corrosion. b) Picture of the 5/95 (wt/wt) $CaCl_2/CaCO_3$ deposit taken immediately after the furnace exposure. This deposit proved to be the most corrosive both in the 72 and 168-hour tests at 80 °C. Given the low amount of hygroscopic $CaCl_2$ in the mixture, a wet solution had not formed (see 100 wt% $CaCl_2$ in Fig. 11b).

A 168-hour test at 120 °C and 20 vol% H_2O (not mentioned in Table 4) was carried out using carbon steel (P235GH) samples without prewetting the salt deposit (5 wt% $CaCl_2$/ 95 wt% $CaCO_3$). The salt deposit was completely dry after the exposure, and no sign of corrosion was found. This test was done to prove that dry $CaCl_2$ is not corrosive above the deliquescence curve if it does not absorb water.

3.3. Corrosion mechanisms

One steel with the salt deposit per experimental condition was incapsulated in epoxy resin to study the corrosion reactions from the cross-section using SEM-EDX. A SEM image of the carbon steel sample exposed to 5/95 (w/w) $CaCl_2/CaCO_3$ mixture at 80 °C and 20 vol% H_2O is illustrated in Fig. 15**a.** Fig. 15**b** presents EDX analyses of selected spots close to a corrosion pit.

Spots 1 and 2 located close to the steel surface have high Cl (4.8 and 5.7 atomic%) and low Ca contents. When $CaCl_2$ deliquesces, the salt dissociates according to the following reaction:

$$CaCl_2\ (aq) \rightarrow Ca^{2+}\ (aq) + 2\ Cl^-\ (aq) \quad (2)$$

Further, when iron is dissolved, the Fe^{2+}(aq) ions attract Cl^- to form $FeCl_2$(s, aq), i.e., a corrosive and hygroscopic compound. Furthermore, $FeCl_2$ in water leads to the hydrolysis reaction forming iron hydroxide and hydrochloric acid according to the following reaction [23]:

$$FeCl_2\ (s, aq) + 2H_2O(l) \rightarrow Fe(OH)_2\ (s) + 2H^+(aq) + 2Cl^-(aq) \quad (3)$$

The HCl formed in reaction (3) lowers the local pH and Cl^- can be recycled back to the steel surface. This process is referred to as auto-catalytic corrosion reaction [23]. Outside the corrosion pit (Area 4 of Fig. 15), the chlorine concentration is significantly lower.

Fig. 16 illustrates the upper corrosion layer.

Spot analyses of Area 1 and 2 in the picture (Fig. 16**a**) show high oxygen and iron content (Fig. 16**b**), this suggests the presence of corrosion compounds such as iron oxides and/or iron hydroxide. These compounds are responsible for the red brownish colour (hematite or Fe $(OH)_3$) that was observed following the furnace exposure (see Fig. 14**b**). Area 3 (Fig. 16) is mainly a mixture of $CaCl_2$ and $CaCO_3$.

4. Summary and conclusions

This work explored the corrosive effects of deliquescent calcium chloride on carbon steel used in the cold-end parts of boilers. Full-scale measurements in a biomass BFB boiler were performed with corrosion/deposit probes in the air preheater area. Furthermore, tests in a

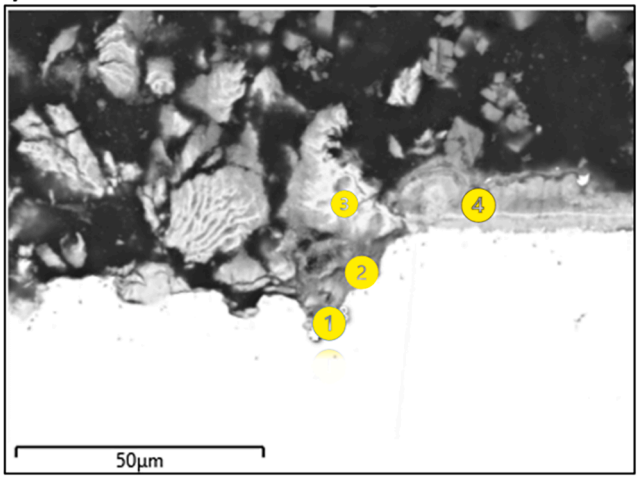

b)

Atomic %

Area	O	Fe	Cl	Ca	O/Fe
1	46.9	47.7	4.8	/	0.98
2	45.8	47.7	5.7	0.2	0.96
3	60.3	37.2	1.3	0.7	1.62
4	62.4	32.5	0.8	4	1.92

Fig. 15. a) Cross-section SEM image of the surface of a carbon steel (P235GH) sample exposed to a 5/95 (wt/wt) $CaCl_2/CaCO_3$ deposit at 80 °C for one week. Feed gas composition during exposure: 20 vol% H_2O, 5 vol% O_2, 75 vol% N_2. b) EDX elemental analyses of different spots.

a)

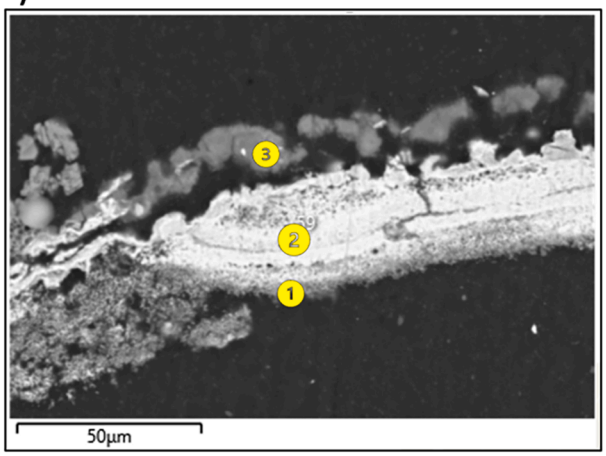

b)

Atomic %

Area	O	Fe	Cl	Ca	O/Fe
1	61.4	33.5	2.6	1.5	1.83
2	56.2	40.7	1.7	1.3	1.38
3	59.8	0.9	19.2	20.1	/

Fig. 16. a) Cross-section SEM image of an upper corrosion layer. Image taken from the same sample of Fig. 15. b) EDX elemental analyses of selected spots.

laboratory furnace have been performed to study the low-temperature corrosion caused by different $CaCl_2$-$CaCO_3$ mixtures on carbon steel (P235GH) and stainless steel (AISI304L).

Both the laboratory tests and the full-scale measurements showed that the corrosion rate of carbon steel is high (>1 mm/year) when deliquescence occurs. Tests performed with supersaturated $CaCl_2$ at 100 and 120 °C, between the deliquescence and the recrystallization of calcium chloride, showed less corrosion than the ones at lower temperature (80 °C). The furnace tests in the laboratory utilizing mixtures of $CaCl_2$ and $CaCO_3$ have shown that calcium chloride is very corrosive on carbon steel even when it comprises just a small percentage (5 wt%) of the salt mixture.

To avoid heavy corrosion by hygroscopic $CaCl_2$, the deposit/material temperatures should be kept above the deliquescence temperature. The increase of the moisture levels in the flue gas during boiler operations needs to be taken into account in order to anticipate $CaCl_2$-induced corrosion. When the water vapor content in the flue gas is high, due to soot blowing or wet fuel, $CaCl_2$ can absorb moisture and remain corrosive even when the water vapor drops back to lower levels.

Future experiments in the laboratory furnace to study the corrosivity of $CaCl_2$ could include the use of HCl and CO_2 in addition to H_2O in the feed gas to better simulate the conditions that occur in a full-scale boiler.

CRediT authorship contribution statement

Alessandro Ruozzi: Investigation, Visualization, Writing – original draft. **Emil Vainio:** Supervision, Conceptualization, Funding acquisition, Writing – review & editing. **Hanna Kinnunen:** Investigation, Writing – review & editing. **Leena Hupa:** Writing – review & editing.

Declaration of Competing Interest

The authors declare that they have no known competing financial interests or personal relationships that could have appeared to influence the work reported in this paper.

Data availability

Data will be made available on request.

Acknowledgements

Funding from the Graduate School at Åbo Akademi is gratefully acknowledged. Support by the Academy of Finland (Properties and behaviour of deliquescent salts and deposits in biomass and waste thermal conversion - Towards improved efficiency and reliability, Decision No. 333917) is also gratefully acknowledged. In addition, the support from the CLUE^2-project partners Andritz Oy, Valmet Technologies Oy, UPM-Kymmene Oyj, Metsä Fibre Oy, and International Paper Inc., are gratefully acknowledged. We want to thank Linus Silvander for carrying out the SEM/EDX analyses and Jaana Paananen for her help in the laboratory.

References

[1] Vainio E, DeMartini N, Hupa L, Åmand L-E, Richards T, Hupa M. Hygroscopic Properties of Calcium Chloride and its Role on Cold-End Corrosion in Biomass Combustion. Energy Fuels 2019;13:11913–22.
[2] Piper J, Van Vliet H. Effect of temperature variation on composition, fouling tendency, and corrosiveness of combustion gas from a pulverized-fuel-fired steam generator. Trans ASME 1958;80:1251–63.
[3] Mobin M, Malik AU, Al-Hajri MJ. Fail Anal Prevent 2008;8(1):69–74.
[4] Vainio E, Vänskä K, Laurén T, Yrjas P, Zabetta E, Hupa M, et al. Impact of boiler load and limestone addition on SO_3 and corrosive cold-end deposits in a coal-fired CFB boiler. Fuels 2021;304:121313.
[5] Glarborg P, Marshall P. Mechanism, and modelling of the formation of gaseous alkali sulfates. Combust Flame 2005;141(1–2):22–39.
[6] Lisa K, Lu Y, Salmenoja K. Sulfation of Potassium Chloride at Combustion Conditions. Energy Fuels 1999;13:1184–90.
[7] Kassman H, Bäfver L, Åmand L-E. The importance of SO_2 and SO_3 for sulphation of gaseous KCl – An experimental investigation in a biomass fired CFB boiler. Combust Flame 2010;157(9):1649–57.
[8] Hygroscopic $CaCl_2$ corrosion mechanism in the air preheater area of industrial boilers. Alessandro Ruozzi's master thesis, University of Modena and Reggio Emilia, Department of Engineering "Enzo Ferrari", Italy, December 2020.
[9] Vainio E, Kinnunen H, Lauren T, Brink A, Yrjas P, DeMartini N, et al. Low-Temperature Corrosion in Co-Combustion of Biomass and Solid Recovered Fuels. Fuel 2016;184:957–65.
[10] Lindau L, Goldschmidt B. Low temperature corrosion in bark fuelled small boilers; Report No. 2002:781; Varmeforsk Services AB: Stockholm, Sweden, 2002.
[11] Retschitzegger S, Brunner T, Obernberger I. Low-Temperature Corrosion in Biomass Boilers Fired with Chemically Untreated Wood Chips and Bark. Energy Fuels 2015;29(6):3913–21.
[12] Herzog T, Müller W, Spiegel W, Brell J, Molitor D, Schneider D. Corrosion caused by dewpoint and deliquescent salts in the boiler and flue gas cleaning VGL: KG Thome-Kozmiensky og M. Beckmann: Energie aus Abfall Band 9 Neuruppin: TK Verlag **2012**, 429–460.
[13] Vainio E, Lauren T, DeMartini N, Brink A, Hupa M. Understanding low-temperature corrosion in recovery boilers: risk of sulphuric acid dew point corrosion? J Sci Technol For Prod Processes 2014;4(6):14–22.
[14] Brunner T, Reisenhofer E, Obernberger I, Kanzian W, Forstinger M, Vallant R. Low-Temperature Corrosion in Biomass Fired Combustion Plants - Online Measurement of Corrosion Rates, Acid Dew Points and Deliquescence Corrosion, 25th European Biomass Conference and Exhibition, Stockholm. Sweden 2017. https://doi.org/10.5071/25thEUBCE2017-2AO.8.1.
[15] DeMartini N, Vainio E, Lauren T, Hupa L. Bisulfate Formation and Impact on Low Temperature Corrosion in Kraft Recovery Boilers, International Chemical Recovery Conference, Halifax, Canada, **2017**.
[16] DeMartini N, Vainio E, Holmblad H, Hupa M. Understanding low temperature corrosion in Kraft Recovery Boilers – Implications for Increased Energy Recovery, Pulping, Engineering, Environmental, Recycling, Sustainability. (PEERS) Conference, Jacksonville, Florida, USA Proceedings, **2016** Tang.

[17] I. N Munkelwitz H. R. Composition and temperature dependence of the deliquescence properties of hygroscopic aerosols. Atmospheric Environment **1993**, 27A(4), 467–473.
[18] Weast RC, editor. Handbook of Chemistry and Physics. Boca Raton, FL: CRC; 1975.
[19] Yang L, Pabalan RT, Juckett MR. Deliquescence Relative Humidity Measurements Using an Electrical Conductivity Method. J Solution Chem 2006;35(4):583–604.
[20] Li X, Gupta D, Eom H-J, Kim H, Ro C-U. Deliquescence and efflorescence behavior of individual NaCl and KCl mixture aerosol particles. Atmos Environ 2014;82: 36–43.
[21] Jozewicz W, Gullett BK. Reaction Mechanisms of Dry CaBased Sorbents with Gaseous HCl. Ind Eng Chem Res 1995;34(2):607–12.
[22] Borgmann CW. Initial Corrosion Rate of Mild Steel Influence of the cation. Ind Eng Chem 1937;29(7):814–21.
[23] Moore JD. Long-term corrosion processes and steel shipwrecks in the marine environment: a review of current knowledge. J Marit Archaeol 2015;10:191–204.